Thermal and energy analysis of DMTA tests

André Chrysochoos, Olivier Arnould

OVERLAY

Journal of Theoretical, Computational and Applied Mechanics

JTCAM

DIAMOND OPEN ACCESS

Identifiers
DOI 10.46298/jtcam.9726
OAI hal-03697346v3

History
Received Jun 22, 2022
Accepted Jan 3, 2023
Published Mar 9, 2023

Associate Editor
Laurence Brassart

Reviewers
Anonymous
Anonymous

Open Review
OAI hal-04021563

Supplementary Material
Data
DOI 10.5281/zenodo.7257481

Thermal and energy analysis of DMTA tests

André Chrysochoos and Olivier Arnould

Laboratoire de Mécanique et Génie Civil, Université de Montpellier, CNRS, Montpellier, France

This paper investigates the suitability of the isothermal linear viscoelastic framework to describe the behavior of polymers observed during DMTA tests. A good interpretation of these tests is important because, in practice, they are used to construct master curves using the time-temperature superposition principle at small strain. These curves are then considered to predict the material behavior under experimentally unreachable thermal and/or loading frequency conditions. Currently, the DMTA protocol neglects the temperature variations induced by the deformation of polymers. We wonder if these temperature variations can have an influence on the measurement of dynamic moduli. To answer this question, quantitative infrared techniques were developed and used to assess small temperature variations of samples undergoing cyclic loadings during mechanical spectrometry tests. Thermal and mechanical data were used to quantify the viscous dissipated and the thermoelastic coupling energies that can be both associated with the hysteretic stress-strain response of polymers. Energy balances were then performed to quantify the relative importance of dissipative and thermoelastic coupling heat sources. From the energy standpoint, it is found that the thermoelastic energy rate was dozens of times higher than the dissipation. Especially at low frequencies, thermoelastic effects can have a greater influence on the loss modulus value than viscosity.

Keywords: DMTA, viscous dissipation, thermoelastic coupling, energy balance, time-dependent behavior

1 Introduction

Dynamic mechanical thermal analysis (DMTA) is widely used in standard experimental approaches developed to characterize the linear viscoelastic behavior of polymers. Samples are subjected to a monochromatic sinusoidal loading (e.g., in tension-compression) and the stress-strain response is recorded at different environmental chamber temperature T_0 and loading frequency f_0, to derive the so-called dynamic moduli E' and E''. According to the hypotheses of DMTA, the storage modulus E' is linked to the stored elastic energy, finally mechanically recoverable when the specimen is unloaded, while the loss modulus E'' is related to the viscous dissipated energy over a loading cycle. In the literature, the viscous part of the behavior is equally quantified by the loss angle δ, defined by $\tan\delta = E''/E'$, which characterizes the so-called internal friction (Menard 2008; Rittel 2000). The DMTA rheological equations for the case of strain-controlled tensile loading can be gathered as follows:

$$\varepsilon = \varepsilon_0 \sin\omega_0 t \tag{1a}$$

$$\sigma = \sigma_0 \sin(\omega_0 t + \delta) = E'(T_0, f_0)\varepsilon_0 \sin\omega_0 t + E''(T_0, f_0)\varepsilon_0 \cos\omega_0 t \tag{1b}$$

$$E'(T_0, f_0) = \frac{\sigma_0}{\varepsilon_0}\cos(\delta(T_0, f_0)) \tag{1c}$$

$$E''(T_0, f_0) = \frac{\sigma_0}{\varepsilon_0}\sin(\delta(T_0, f_0)) \tag{1d}$$

where ε_0 stands for the controlled strain amplitude, $\sigma_0(T_0, f_0)$ the resulting stress amplitude and $\omega_0 = 2\pi f_0$ the pulsation.

Equation (1) forms the theoretical interpretation framework of DMTA. It deserves several comments:

- The mechanical spectrometry tests assume that to a monochromatic mechanical loading corresponds a monochromatic response. Naturally, this crucial preliminary assumption can/should be systematically verified via a frequency spectrum analysis of the loading signal and of the material response. The two questions that need to be imperatively answered are: is the testing machine capable of imposing a monochromatic loading? Is the material response then also monochromatic?
- Moreover, although tests are performed at different temperatures, they are generally considered isothermal, the sample being assumed to be in thermal equilibrium with the environmental chamber. However, the cyclic deformation mechanisms of polymers often lead to temperature variations of the specimen. Material deformation process generates indeed heat sources. Dissipative sources induced by irreversible transformations, due at least to viscosity, must be first mentioned. In addition, it is known that polymer behaviors are sensitive to temperature variations. This sensitivity results in coupling mechanisms, highlighting the strong dependence between thermal, mechanical and microstructural states. One can mention the linear thermal expansion of polymers (Graessley and Fetters 2001), the rubber effects (Treloar 2005), or simply the fact that dynamic moduli vary with temperature (e.g., the temperature T_0 of the DMTA environmental chamber) (Ferry 1980; Menard 2008). Consequently, are the temperature variations of the sample undergoing DMTA testing significant or not? If so, a better understanding of the energy balance of the polymer deformation is then interesting from a rheological standpoint, dissipative mechanisms being closely associated with evolution laws, while coupling effects are linked to state laws (Chrysochoos 2012; Halphen and Nguyen 1975).

The first goal of this paper is to present the thermography setup used to assess very small strain-induced temperature variations occurring during cyclic DMTA tests. As already mentioned, DMTA performs isothermal analysis even if different testing temperatures are, by construction, considered in testing campaigns. This isothermal analysis was reconsidered to check whether the origin of the storage and loss moduli is only due to visco-elastic effects whatever the couple (T_0, f_0). In the following, metrological aspects related to measurements of small temperature variations were thoroughly presented. Indeed, the first experimental challenge was to measure these strain-induced temperature variations. Even if these temperature variations remain often much smaller than a tenth of a degree, they may correspond to heat rates much greater (e.g., dozens of times) than the deformation energy rate (Boulanger et al. 2004). More precisely, we noticed in Moreau et al. (2005) that the viscous dissipative effects were energetically negligible compared to the thermoelastic coupling effects by measuring the small temperature variations (< 500 mK) of PMMA and PC specimens, during load-unload tests at low strain rate. It is consequently crucial not to neglect the smallest temperature variation when establishing an energy balance.

2 Experimental setup

The chosen polymers in this study were commercial PS (Polystyrene from Goodfellow) and commercial PA6.6 (Polyamide 6.6, Technyl®A218 provided by Solvay Engineering Plastics). The specimens of dimension $85 \times 13 \times 4$ mm were machined from thick sheets of 300×300 mm. The glass transition temperatures T_g were measured using modulated reversed calorimetry in a differential scanning calorimeter (Mettler Toledo DSC-3) at a heating rate of 2 K/min up to 473 K. They are reported in Table 1. We chose to define T_g as the onset temperature at the inflection point temperature during the DSC measurements. In the case of PA6.6, the sample water content has a great influence on T_g value and consequently on the mechanical response (Benaarbia et al. 2016; Fabre et al. 2018; Launay et al. 2013). In our case the samples were stored in the air-conditioned room (i.e., regulated in temperature and humidity) of the DMTA. We measured, by weighing and drying in an oven, a water content of about 1–2 %, which agrees with the measured glass transition temperature of 336 K (Batzer and Kreibich 1981; Reimschuessel 1978). It's known that the T_g measured by DMTA could be different than the one measured by DSC (Achorn and Ferrillo 1994; Rieger 2001) and depends at least on the loading frequency. In all our DMTA measurements, we expected to be always below T_g, as can be seen later on the $\tan\delta$ curves in Figure 4. Thermal expansion coefficient and specific heat values, which were extracted from the

technical literature, are reported in Table 1 too. All these values may vary slightly from one reference to another, sometimes due to difference in molecular weight.

Table 1 Thermophysical parameters of the PS and PA6.6 samples.

	T_g [K]	ρ [kg/m^3]	C [J/kg/K]	λ_{th} [10^{-6} /K]
PS	375	1060	1400	75
PA6.6	336	1140	1800	85

2.1 Thermal metrology

The experimental setup is shown in Figure 1. Temperature variations were observed using an infrared focal plane array (IRFPA) camera (CEDIP Titanium series). The environmental chamber of the DMTA (Bose ELF 3230) was equipped with a home-made door using an infrared Techspec lens (EDMUND optics) and placed at the center of the door. This infrared lens was made of anti-reflecting coated silicon to avoid IR reflections and was suitable for the DMTA measurements in the wavelength range of 3-5 µm (transmission coefficient of IR radiations in this range remains greater than 93 %).

Figure 1 Thermography setup in front of the DMTA.

This infrared lens was thus able to capture the temperature variations observed during the tests by weakly attenuating them. Note that the Narcissus effect has been ruled out by slightly misaligning the camera from the IR lens axis. Furthermore, two samples were placed inside the environmental chamber, in the optical field of the IRFPA camera and at the same focal plane, one sample being subjected to the loading and the other one mechanically free (dummy sample) and submitted to the thermal regulation of the environmental chamber (Figure 2).

Figure 2 Thermal image [°C] of the two PS samples inside the environmental chamber at 50 °C.

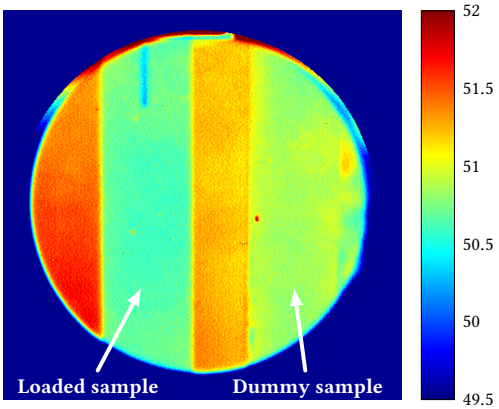

The IRFPA camera was calibrated using a pixel-by-pixel method (Honorat et al. 2005). This pixel calibration is an effective technique for quantitatively reliable infrared measurements of

temperature fields, particularly when very small temperature variations occur. This type of calibration allows the user to by-pass the "bad pixel replacement" (BPR) and "non uniformity correction" (NUC) stages proposed by some camera's builders. The individual pixel calibration is done on the entire dynamic range of the sensor and is based on polynomial fitting of the digital levels s_i delivered by the i^{th} element of the detector matrix when the camera is placed in front of a black body source at different temperatures $T \in [T_1, T_2]$:

$$s_i(T) = \sum_{p=0}^{P} a_{ip} T^p, \quad T \in [T_1, T_2] \tag{2}$$

where the coefficients a_{ip} derive from a least squares fitting. Later, the system will consider pixel i as a bad pixel based on the temperature difference between the temperature predicted by the polynomial fitting and the imposed temperature of the black body source. If this difference is greater than a predefined threshold of δT (e.g., $\delta T = 10\,\text{mK}$), the pixel is considered as bad (Honorat et al. 2005).

This calibration procedure was adopted for each testing temperature T_0 used to ensure that very small strain-induced temperature variations of the sample are measured. Calibrations were performed before each mechanical test series, using the black body behind the environmental chamber's door with the IR lens and using the same geometrical configuration as during the DMTA test, the surface of the black body being at the same position as the sample surface. The integration time was varied according to the temperature used during the DMTA tests. To avoid transient thermal drifts of the camera, these calibrations and measurements were performed about 4-5 hours after switching on the camera.

A tricky recurrent problem associated with the IR thermal measurements is the emissivity of the target, here the emissivity of the sample surface. It was verified whether painting the sample black will affect the emissivity of the sample, as some samples (PS) were transparent to the visible radiations. Therefore, half of one PS sample was painted black and half of it was left unpainted. Using the experimental setup shown in Figure 1, thermoelastic responses were analyzed over the sample gauge part to check if painting the sample black makes a difference in the emissivity (in the IR wavelengths) of the sample. The thermoelastic field of temperature amplitudes was plotted over the region of interest including both sides (i.e., painted and unpainted). It was observed that painting the sample in black induced a more homogeneous thermoelastic signal but did not significantly affect its mean amplitude over the sample gauge part. We consequently decided to leave the sample surfaces unpainted.

2.2 Mechanical loadings

Regarding now the loading aspects of the cyclic tests, we limited the mechanical tests to three decades of loading frequencies for different environmental chamber's temperatures, all below the glass transition temperature T_g to limit the complexity of the behavior to that of glassy polymers.

In this work, a complete calibration of the load cell and of the LVDT displacement sensor were performed. Moreover, the alignment of the clamps was verified and adjusted to ensure a pure tensile loading of the sample. For this purpose, we used a PS sample equipped with four strain gauges, two by side, to verify if the strain is (almost) equal for all the four gauges for different applied quasistatic load in tension and compression until the maximum load. In addition, the DMTA electronic acquisition chain influenced the phase shift between the imposed displacement and the measured force. This phase shift was corrected in the (commercial) software but, as we used the raw data to fully control the data processing and to synchronize these signals with the IR camera acquisition, an electronic phase shift correction has been done on the raw data. This phase shift has been evaluated at all the measured frequencies and at two temperatures (28 °C and 60 °C) using a sample of steel (no material viscosity) sheet. This steel sheet was of the same length as the polymer samples but with a cross-section area such that it has a stiffness equivalent to that of PS samples. Finally, regarding the real sample elongation, it was considered that components of the DMTA machines (especially the load cell) induced a non-negligible spurious displacement that induced an important bias. Therefore, the machine stiffness was measured using a very stiff sample. The actual elongation of the sample was then obtained by

correcting the machine displacement from its own deformation. This was checked by measuring the actual displacement, during cyclic loadings, between two targets on the surface of a polymer sample by digital image correlation (Wattrisse et al. 2001) using IR thermal images. The polymer samples complex stiffness was then corrected following (Olusanya 1996, Eq. (16A)). The moduli determined on the PS and PA6.6 samples were compared with measurements obtained on similar samples using other DMTA in three other French laboratories (Yadav 2019).

The raw displacement and load measurements of the DMTA were used to verify the monochromatic character of the loading and response signals. An example of the Fourier spectrum of the raw signals, recorded on a PS sample at 1 Hz, is shown in Figure 3.

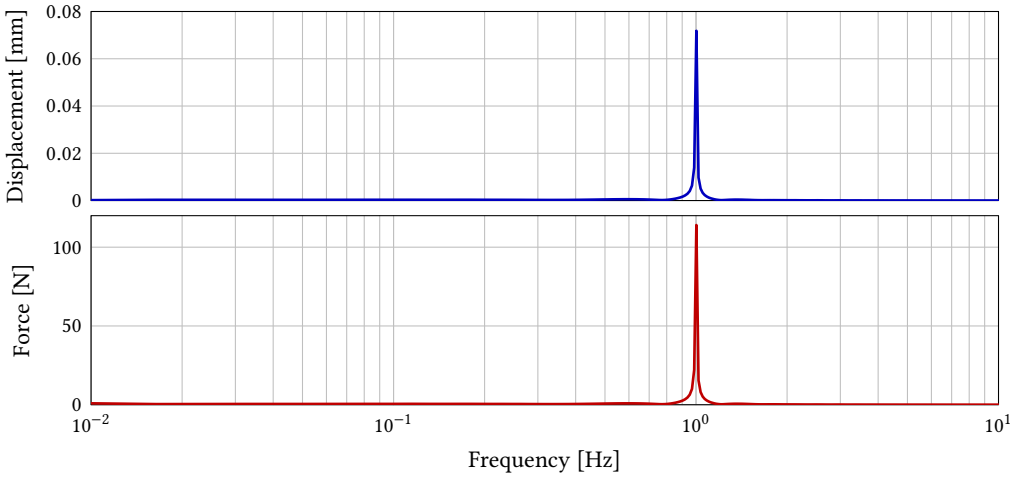

Figure 3 Frequency spectrum of the force and displacement signals for PS sample at a loading frequency of 1 Hz and a temperature of 40 °C.

This type of control was performed on all samples, regardless of the loading frequency f_0 or the ambient temperature T_0 at which the test was performed. Strain controlled tension-compression symmetric cyclic measurements were conducted on specimens at several frequencies (e.g., 0.01, 0.1, 1 and 10 Hz) and several temperatures. The following sets of T_0 have been particularly analyzed: (313 K, 348 K, 363 K) for the PS samples and (313 K, 323 K, 333 K) for the PA6.6 samples. Note that a new sample was used after each frequency sweep, i.e., for each new temperature T_0, to reduce aging effects or change in water content.

The recordings were made over several tens of cycles to get a stabilized cyclic regime and ensure a sufficient set of mechanical and thermal data to perform relevant filtering. We used the same sampling frequency whatever the loading parameters and the polymer tested. This sampling frequency f_s was set at 31 Hz, as a unique electronic sampler being used to record thermal and mechanical data synchronously. This sampling frequency is large enough for loading frequencies below 1 Hz. In fact, whatever the loading frequency, the expected periodicity of the signal, once the transient period is over, allowed us to analyze the thermal response via synchronous demodulation techniques. In addition, the sampling frequency of 31 Hz was chosen so as not to be an integer multiple of the high loading frequencies used of 6.3 and 10 Hz (under-sampling technique). The loading parameters used during the different tests are mentioned in Table 2.

Table 2 Loading parameters of DMTA tests.

	Polystyrene	Polyamide 6.6
Maximum strain [%]	0.1	0.1
Strain ratio	−1	−1
Frequency range [Hz]	0.01–10	0.01–10
Temperature range [K]	313–363	308–333

3 Results and Discussion

The results obtained were processed separately: on the one hand, mechanical data (load, displacement, time) led us to identify dynamic moduli, see Equations (1c) and (1d), as functions of the testing temperature T_0 and of the loading frequency f_0; on the other hand, IR data gave us the temperature variations of the specimen inside the environmental chamber due to the cyclic loading.

3.1 Estimates of dynamic moduli E' and E''

Classically, DMTA is used to identify the evolution of dynamic moduli. All devices directly provide E' and E'' moduli (or equivalently E' and $\tan\delta$), as they are equipped with a specific processing data software. In the present case, we decided to process the raw stress and strain data recorded as a function of time, the dynamic moduli have thus been estimated using a simple least-squares method of the stress and strain signals.

Series of frequency sweeps gave the evolution of E' and E'' shown in Figure 4 and presented as functions of the loading frequency f_0 and environmental chamber temperature T_0. These data were extracted from (Yadav 2019).

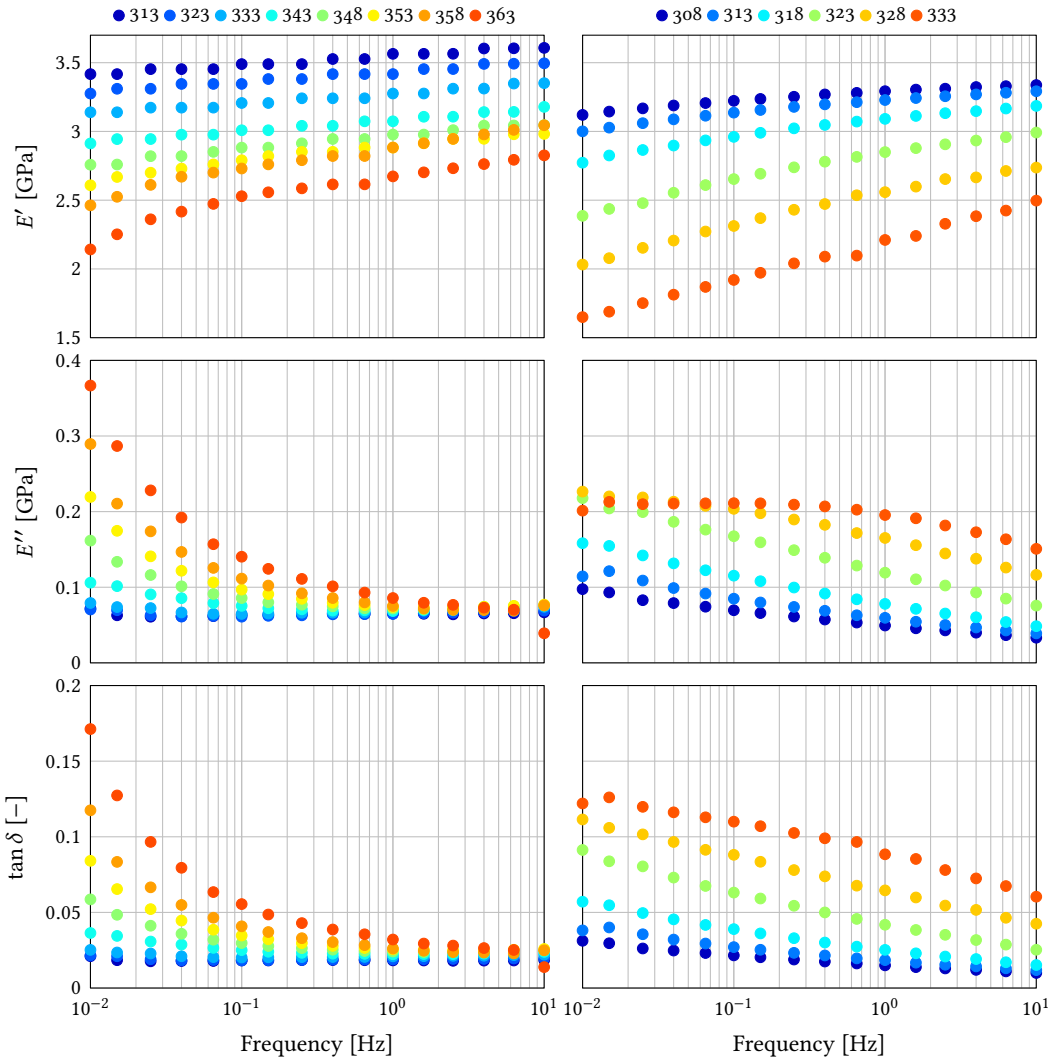

Figure 4 Influence of frequency and temperature on dynamic moduli and $\tan\delta$ of PS [left] and PA6.6 [right], after (Yadav 2019); colors indicate the temperature T_0 [K] of the environmental chamber.

It was observed that the evolution of E' and E'' have the same trends for both materials (PS and PA6.6): for the used frequency range, E' is increasing with the increasing frequency whereas E'' is decreasing. On the other hand, an increase in the testing temperature will tend to decrease the storage modulus and increase the loss modulus. Finally, it is worth mentioning the difference

in the order of magnitude between E' and E'', loss moduli being, roughly speaking, dozens of times weaker than storage moduli.

Naturally, this type of result is very common in the literature and widely used in the polymer material characterization centers to construct master curves associated with the famous, and sometimes controversial, time-temperature superposition principle (Sokolov and Hayashi 2007). However, if the mechanical data from DMTA tests are abundant, the associated thermal responses have not, to our knowledge, been analyzed yet. This is probably not surprising since, as previously underlined, one of the implicit assumptions of DMTA tests is to consider that the sample is in thermal equilibrium with the environmental chamber inside which it is cyclically loaded.

3.2 Analysis of temperature variations

To estimate the so-called "temperature variations of the sample" $\theta(t)$, we used the infrared techniques presented in Section 2.1. These temperature variations were defined by the difference between the average temperatures estimated over two small areas of $2 \times 2\,\mathrm{mm}^2$ placed, one in the center of the sample being deformed and, the other, in the center of the dummy sample, see Figure 2. The purpose of calculating an average temperature over a small area is to reduce high frequency thermal noise. For the IRFPA camera used in this work, this noise is white Gaussian noise (Batsale et al. 2013; Chrysochoos and Louche 2000). Considering the temperature difference between the strained sample "$T(t)$" and the dummy sample "T_0" is intended to mitigate the effects of low frequency temperature fluctuations in the environmental chamber induced by its own thermal regulation system.

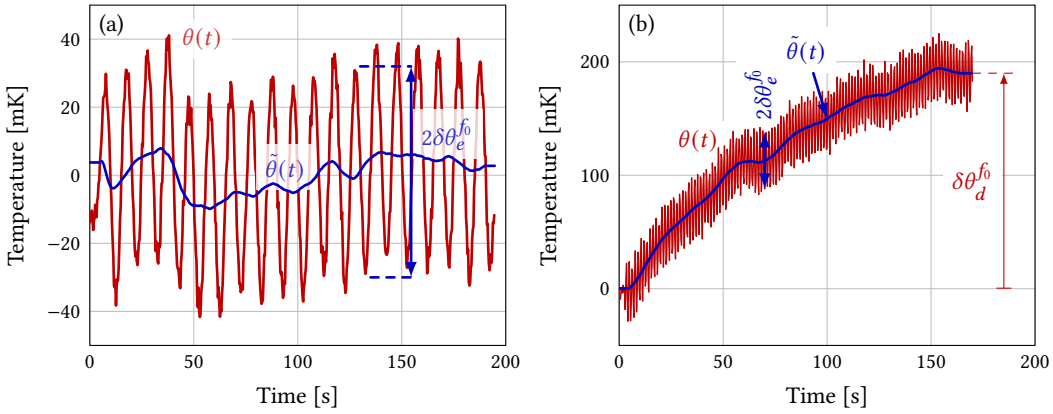

Figure 5 Time histories of $\theta(t)$: (a) PA6.6, $T_0 = 313\,\mathrm{K}$, $f_0 = 0.1\,\mathrm{Hz}$; (b) PA6.6, $T_0 = 333\,\mathrm{K}$, $f_0 = 10\,\mathrm{Hz}$.

Figure 5 presents the temperature $\theta(t)$ obtained on PA6.6 samples. To fix the ideas we have chosen the couples (313 K, 0.1 Hz) and (333 K, 10 Hz) representing the extreme conditions of mechanical and thermal loading for the polyamide samples. The red curve shows $\theta(t)$ while the blue curve represents the mean temperature per cycle defined by

$$\tilde{\theta}(t) = f_0 \int_{t-(2f_0)^{-1}}^{t+(2f_0)^{-1}} \theta(\tau)\,\mathrm{d}\tau. \tag{3}$$

The difference $\theta(t) - \tilde{\theta}(t)$ highlights regular and periodic oscillations whose amplitude has been noted $\delta\theta_{\mathrm{e}}^{f_0}$. We finally introduced the temperature difference

$$\delta\theta_d^{f_0} = \tilde{\theta}(t_{\mathrm{end}}) \tag{4}$$

where t_{end} is the end time of the camera recording. This temperature allowed us to quantify a potential self-heating of the sample induced by viscous dissipation. However, the value of $\delta\theta_d^{f_0}$ can be affected by the residual temperature fluctuations of the environmental chamber.

These first thermal data allowed us to point out the two following results:

- First, we observed that the temperature variations during the DMTA test remained very small (less than a few hundreds of mK). On the one hand, this result is reassuring in that it is consistent

with the assumption of a DMTA test during which the sample is in thermal equilibrium with the ambient temperature of the environmental chamber. On the other hand, one could be surprised not to see much more significant dissipation-induced self-heating. In the case of Figure 5(a), the loading frequency is low (0.1 Hz) and no significant $\delta\theta_d^{f_0}$ is observed. However, in the case of Figure 5(b), PA6.6 sample is cyclically loaded at 10 Hz at a temperature of 333 K, the temperature increase $\delta\theta_d^{f_0}$ does not exceed 200 mK during the test duration. In the next subsections we checked whether this observation is consistent with the temperature variations induced by viscous dissipation predicted by the rheological Equation (1).

- Even if variations of $\theta(t)$ are small, regular oscillations can be observed which appears to be periodic, and this periodicity is linked to the loading frequency f_0. We noted $\delta\theta_e^{f_0}$ the amplitude of these oscillations and we proposed to associate them with thermoelastic effects. In the next subsection, a thermoelastic rheological equation was introduced to check this proposal.

3.3 Thermodynamic standpoint and energy balance analysis

To go further, it is necessary to consider the 1D rheological equations associated with the DMTA tests and try to integrate them in a thermodynamic framework to be able to draw up a complete energy balance. In this work, the thermodynamics of irreversible processes (TIP) with internal state variables was used (Chrysochoos 2012; Germain et al. 1983; Halphen and Nguyen 1975). This formalism assumes that a local equilibrium state exists and that it can be described by a finite number of state variables. The properties of equilibrium states are described by the state laws derived from a thermodynamic potential. In mechanics of materials, the volume Helmholtz free energy ψ is often used. The state variables are the temperature T, the small strain ε and a given number of complementary (internal) state variables α_j, $j = 1, 2\ldots$, usually introduced to describe the microstructural state of the material. Evolution or complementary equations must also be introduced to describe the irreversibility accompanying the deformation process. The latter must be compatible with the Clausius-Duhem inequality, local writing of the second principle of thermodynamics (Chrysochoos 2012).

Using the rheological Equation (1) associated with the DMTA tests, the stress σ can be rewritten in the following form, easier to interpret from a thermodynamic standpoint:

$$\sigma = E'(T_0, f_0)\varepsilon + \frac{E''(T_0, f_0)}{2\pi f_0}\dot{\varepsilon}. \tag{5}$$

The energy denomination of E' and E'' allows one to split the stress into reversible (energy storage or conservation) and irreversible (loss of energy) parts so that:

$$\sigma^{\mathrm{r}} = \frac{\partial\psi}{\partial\varepsilon} = E'(T_0, f_0)\varepsilon, \tag{6a}$$

$$\sigma^{\mathrm{ir}} = \sigma - \sigma^{r} = \frac{E''(T_0, f_0)}{2\pi f_0}\dot{\varepsilon}. \tag{6b}$$

The conjugate variable of ε is the so-called reversible stress σ^{r}. The term σ^{ir} is the irreversible stress and will act as the thermodynamic force associated with the strain rate in the Clausius-Duhem inequality, see Section 3.3.2.

The presence, in Equations (6a) and (6b), of the thermomechanical loading parameters T_0 or f_0 is a little bit delicate to integrate in a thermodynamic framework. How can these (external loading) parameters act as material state variables? Regarding T_0, it is quite simple, by just replacing the temperature set point of the environmental chamber by the temperature of the sample T. Regarding f_0, we proposed the following state variable $\tilde{f}$, depicting a memory of kinematic effects accumulated over a time corresponding to a loading duration $\mathcal{T}_0$:

$$\tilde{f} = \frac{1}{2\pi}\sqrt{\frac{\langle\dot{\varepsilon}^2\rangle}{\langle\varepsilon^2\rangle}} \tag{7}$$

where the mean square strain rate and the mean square strain over $\mathcal{T}_0$ are respectively defined by

$$\langle\dot{\varepsilon}^2\rangle = \frac{1}{\mathcal{T}_0}\int_{t-\mathcal{T}_0}^{t}\dot{\varepsilon}^2(\tau)\,\mathrm{d}\tau \quad \text{and} \quad \langle\varepsilon^2\rangle = \frac{1}{\mathcal{T}_0}\int_{t-\mathcal{T}_0}^{t}\varepsilon^2(\tau)\,\mathrm{d}\tau. \tag{8}$$

Naturally, when $\mathcal{T}_0$ corresponds to the cycle period f_0^{-1}, all is done to get $\tilde{f} = f_0$ for a monochromatic loading cycle.

In what follows, we therefore admitted that the free energy ψ was a state function of T, ε and of the history variable $\tilde{f}$ so that $\psi = \psi(T, \varepsilon, \tilde{f})$.

The form of Equation (5) suggests a rheological behavior where elastic effects develop in parallel with viscous effects. Both types of mechanism use the same kinematic variable ε, as does the Kelvin-Voigt model (Aklonis and Mac Knight 1983), with the main difference that here the elasticity and viscosity parameters depend on T and $\tilde{f}$. In the literature, more general models, than the Kelvin-Voigt one, are mentioned, namely the Generalized Maxwell model which allows one to consider the evolution of E' and E'' via a multitude of viscoelastic branches placed in parallel (Aklonis and Mac Knight 1983). For each viscoelastic branch, a viscous strain is necessarily introduced as a state variable. For simplicity in what follows, we have tried to stay as close as possible to the rheological Equation (1) of the DMTA.

3.3.1 Thermoelastic effects

Modeling aspects The regular and periodic thermal oscillations experimentally observed, henceforth referred to as $(\delta\theta_e^{f_0})_{exp}$, led us to introduce thermoelastic effects. In this context, we proposed to rewrite Equation (6a) in the form

$$\sigma^r = E'(T_0, f_0)(\varepsilon - \lambda_{th}\theta) \tag{9}$$

where λ_{th} is the coefficient of thermal expansion. For a thermoelastic material, this strong thermomechanical interaction results in the existence of a coupling heat source written as (Chrysochoos 2012)

$$w^\bullet_{the} = T\frac{\partial^2\psi}{\partial T\partial\varepsilon}\dot{\varepsilon} + T\frac{\partial^2\psi}{\partial T\partial\tilde{f}}\dot{\tilde{f}} = T\frac{\partial\sigma^r}{\partial T}\dot{\varepsilon} + 0 = -\lambda_{th}TE'\dot{\varepsilon} - T\frac{dE'}{dT}(\varepsilon - \lambda_{th}\theta)\dot{\varepsilon}. \tag{10}$$

The notation $(-)^\bullet$ means that the rate of $(-)$ depends on the thermodynamic path followed. In other words, $(-)$ is not a state function. Note that the term in $\dot{\tilde{f}}$ vanishes for any monochromatic cycle ($\tilde{f} = f_0$) so that $w^\bullet_{the}$ finally contains only two terms. The first term is well known. It causes a material to expand when heated or to cool when stretched. The second term is due to the variation of E' with the temperature. If we admit that the derivative dE'/dT remains constant during a DMTA test, the corresponding source should beat at $2f_0$, since ε, $\dot{\varepsilon}$, and, to a good approximation θ, beat at f_0, see for instance Figure 5(a). Indeed, from an experimental standpoint, it was not possible, as shown below, to experimentally see any component of the thermo-signal beating at the frequency $2f_0$, which should have been the case if the second source term had a large amplitude. This is the reason why we have considered, in what follows, a thermoelastic source reduced to the first term with $T \approx T_0$ as $\theta \ll T_0$:

$$w^\bullet_{the} \approx -\lambda_{th}T_0E'(T_0, f_0)\dot{\varepsilon}. \tag{11}$$

To pass from heat sources to temperature variations, the heat diffusion equation is required. For simplicity, we have used in the following a differential version of the heat diffusion equation valid for homogeneous tests when the boundary heat exchange conditions are linear (Fourier conditions) (Chrysochoos and Louche 2000). In such a context, the volume heat losses by conduction were modelled by a linear term in temperature variation weighted by a time constant of heat losses $\tau_{th} = \frac{\rho Ce\ell}{2h(e+\ell)}$ where ρ is the mass density, C, the specific heat of the material (Table 1), e, the sample thickness, ℓ, its width and h, the heat exchange coefficient between the sample and the surroundings. When only the thermoelastic source is considered, this heat equation can be written as (Boulanger et al. 2004)

$$\frac{d\theta}{dt} + \frac{\theta}{\tau_{th}} = \frac{w^\bullet_{the}}{\rho C}. \tag{12}$$

The time constant of thermal return τ_{th} can be experimentally identified for each material by measuring the thermal disequilibrium $T - T_0$ over time during a given thermal loading $T_0(t)$.

During these thermal loading, it was assumed that no heat source was present in the second member of Equation (12). Figure 6 shows an illustration of the quality of the inverse identification procedure using a numerical integration of Equation (12) and a least squares minimization. The identified values were $\tau_{\text{th}} = 48$ s for PS and $\tau_{\text{th}} = 34$ s for PA6.6.

Figure 6 Measured and adjusted temperature for the estimation of τ_{th} for PS sample.

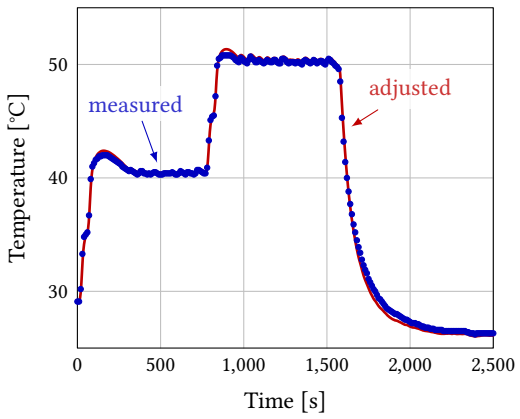

The integration of Equation (12) with thermoelastic source defined in Equation (11), gives, once the transient terms have vanished:

$$\theta_{\text{the}}(t) = -\chi(\omega_0)\frac{\lambda_{\text{th}} T_0 E'}{\rho C}\varepsilon_0 \sin(\omega_0 t + \phi_{\text{the}}) \quad \text{with} \quad \chi(\omega_0) = \frac{\omega_0 \tau_{\text{th}}}{\sqrt{1+\omega_0^2 \tau_{\text{th}}^2}} \tag{13}$$

where $\tan\phi_{\text{the}} = 1/(\omega_0\tau_{\text{th}})$. The amplitude of thermal oscillations of thermoelastic origin $\delta\theta_{\text{e}}^{f_0}$ can therefore be related theoretically to the strain amplitude ε_0 by the relationship

$$(\delta\theta_{\text{e}}^{f_0})_{\text{theo}} = \chi(\omega_0)\frac{\lambda_{\text{th}} T_0}{\rho C} E' \varepsilon_0. \tag{14}$$

As soon as $\omega_0\tau_{\text{th}}$ becomes larger than 1 (e.g., high frequency test, high time constant of heat losses which means that, over one cycle duration, the test can be considered as adiabatic), $\chi \approx 1$ and the above expression can be simplified in $(\delta\theta_{\text{e}}^{f_0})_{\text{theo}} = \frac{\lambda_{\text{th}} T_0}{\rho C} E' \varepsilon_0$. This last expression is often used in the field of thermal stress analysis (Dulieu-Barton and Stanley 1998), since $E'\varepsilon_0$ roughly represents the stress amplitude σ_0. Indeed, noting that σ_0 is reached when the stress rate cancels, it can be shown from Equation (1b) that

$$\sigma_0 = E'\varepsilon_0\sqrt{1+\left(\frac{E''}{E'}\right)^2} = \frac{E'\varepsilon_0}{\sin(\arctan(E'/E''))} \tag{15}$$

which remains close to $E'\varepsilon_0$ if the ratio $E''/E' = \tan\delta$ remains very small compared to 1, which has been the case for the two studied materials, see Figure 4.

Comparison between experimental and predicted data Using Equation (14), an estimate of $(\delta\theta_{\text{e}}^{f_0})_{\text{theo}}$ has been performed for each DMTA test characterized by a (T_0, f_0) couple and compared with the experimental one $(\delta\theta_{\text{e}}^{f_0})_{\text{exp}}$ obtained using a synchronous demodulation of the signal $\theta(t)$.

To check the efficiency of the synchronous demodulation to estimate $(\delta\theta_{\text{e}}^{f_0})_{\text{exp}}$, we compared the difference $\theta(t) - \tilde{\theta}(t)$ with the signal $(\delta\theta_{\text{e}}^{f_0})_{\text{exp}} \sin(\omega_0 t + \phi_{\text{e}})$, where ϕ_{e} is the phase shift of the temperature signal with the carrier signal. As an example, both signals were partly plotted in Figure 7 in the case of the test shown in Figure 5(a) from $t = 85$ s to $t = 110$ s.

We also performed a synchronous demodulation of the thermo-signal $\theta(t)$ at $2f_0$, to check if the amplitude $(\delta\theta_{\text{e}}^{2f_0})_{\text{exp}}$ of $\theta(t)$ induced by the second term of the thermoelastic heat source was significant or not.

The mechanical and thermal data processing was therefore carried out following tests performed on the two materials at different ambient temperatures T_0 and different loading frequencies f_0. The corresponding results were gathered in Table 3(a) for the PS and Table 3(b)

Figure 7 Efficiency of the synchronous demodulation to reach $(\delta\theta_e^{f_0})_{\text{exp}}$ (PA6.6, $T_0 = 313\,\text{K}$, $f_0 = 0.1\,\text{Hz}$, Figure 5(a)).

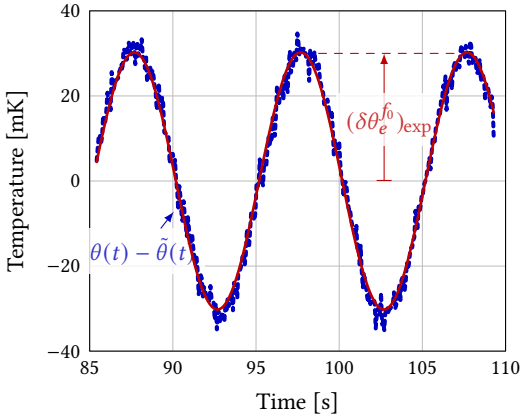

f_0 [Hz]	T_0 [K]	E' [MPa]	χ [-]	$(\delta\theta_e^{f_0})_{\text{theo}}$ [mK]	$(\delta\theta_e^{f_0})_{\text{exp}}$ [mK]	$(\delta\theta_e^{2f_0})_{\text{exp}}$ [mK]
0.1	313	3490	0.999	51	45	1.1
1	313	3560	1.0	53	48	0.3
10	313	3610	1.0	53	43	2.4
0.1	348	2880	0.999	47	41	0.9
1	348	2980	1.0	48	42	0.6
10	348	3050	1.0	50	40	0.9
0.1	363	2530	0.999	43	42	1.6
1	363	2670	1.0	46	41	0.3
10	363	2830	1.0	48	36	0.2

(a) PS samples

f_0 [Hz]	T_0 [K]	E' [MPa]	χ [-]	$(\delta\theta_e^{f_0})_{\text{theo}}$ [mK]	$(\delta\theta_e^{f_0})_{\text{exp}}$ [mK]	$(\delta\theta_e^{2f_0})_{\text{exp}}$ [mK]
0.1	313	3140	0.999	41	30	0.3
1	313	3230	1.0	42	27	0.2
10	313	3290	1.0	43	30	0.1
0.1	323	2650	0.999	35	29	0.5
1	323	2850	1.0	38	27	0.0
10	323	2990	1.0	40	30	0.9
0.1	333	1920	0.999	26	24	0.2
1	333	2210	1.0	30	23	0.0
10	333	2500	1.0	34	26	0.1

(b) PA6.6 samples

Table 3 Temperature variations induced by thermoelasticity for PS. Comparison of measured amplitudes $(\delta\theta_e^{f_0})_{\text{exp}}$ with the predictions of the thermoelastic model $(\delta\theta_e^{f_0})_{\text{theo}}$. Estimates for $(\delta\theta_e^{2f_0})_{\text{exp}}$ are not significant.

for the PA6.6. Note that we limited the frequency range to $[0.1, 10]$Hz, for which the thermal signal remains significant.

Tables 3(a) and 3(b) show that the observed thermoelastic effects are rather correctly predicted by Equation (14). Note that, to compute the predictions of the thermoelastic model, E' assessments were used as well as values of several thermophysical parameters characterizing the material, see Table 1.

Partial concluding comments Comments that can be drawn from this data analysis are:

- Regarding the thermoelastic couplings induced by the variation of the storage modulus, i.e., $-T\frac{\mathrm{d}E'}{\mathrm{d}T}(\varepsilon - \lambda_{\text{th}}\theta)\dot{\varepsilon}$ in Equation (10), they remained undetectable. The values of $(\delta\theta_e^{2f_0})_{\text{exp}}$ shown in Tables 3(a) and 3(b) are too low to be significant.
- Thermoelastic effects induced by material expansion occur during a DMTA test and should probably be considered in the rheological equations. Indeed, it is possible to introduce thermoelastic contributions $E'_{\mathcal{T}}$ and $E''_{\mathcal{T}}$ to the standard dynamic moduli $E'_{\mathcal{M}}$ and $E''_{\mathcal{M}}$ considering the coupling effects beating at the loading frequency f_0. Using Equations (6b), (9) and (13), we then get

$$E' = E'_{\mathcal{M}} + E'_{\mathcal{T}} = E'_{\mathcal{M}} + \frac{\lambda_{\text{th}}^2 T_0 {E'_{\mathcal{M}}}^2}{\rho C}\frac{\omega_0^2\tau_{\text{th}}^2}{1+\omega_0^2\tau_{\text{th}}^2}, \tag{16a}$$

$$E'' = E''_{\mathcal{M}} + E''_{\mathcal{T}} = E''_{\mathcal{M}} + \frac{\lambda_{\text{th}}^2 T_0 {E'_{\mathcal{M}}}^2}{\rho C}\frac{\omega_0\tau_{\text{th}}}{1+\omega_0^2\tau_{\text{th}}^2}. \tag{16b}$$

Tables 4(a) and 4(b) show that the thermoelastic contributions to E' and E'' remained weak, particularly at high frequency. Indeed, at high frequency, the heat losses per cycle drastically decrease and the thermoelastic deformation process becomes adiabatic (no thermal dissipation). Conversely, at low or even very low frequency, we know that the loss moduli E'' tend towards zero, so we can question the relative importance of thermoelastic effects even if, at very low frequencies, the deformation process tends towards an isothermal process. From an experimental

standpoint, these low frequencies are beyond the reach of the infrared techniques currently used. Nevertheless, numerical tests can be performed to check the possible preponderance of thermoelastic effects. The corresponding results will be shown in Section 3.3.5 once the dissipative effects and energy balances have been introduced and analyzed.

f_0 [Hz]	T_0 [K]	E' [MPa]	E'' [MPa]	$E'_{\mathcal{T}}$ [MPa]	$E''_{\mathcal{T}}$ [MPa]
0.1	313	3490	67	12.6	0.42
1	313	3564	65	13.1	0.04
10	313	3608	64	13.5	0.00
0.1	348	2882	86	9.5	0.32
1	348	2977	77	10.2	0.03
10	348	3046	73	10.7	0.00
0.1	363	2529	140	7.7	0.25
1	363	2673	86	8.6	0.03
10	363	2826	39	9.6	0.00

(a) PS samples

f_0 [Hz]	T_0 [K]	E' [MPa]	E'' [MPa]	$E'_{\mathcal{T}}$ [MPa]	$E''_{\mathcal{T}}$ [MPa]
0.1	313	3137	85	10.8	0.51
1	313	3228	60	11.5	0.05
10	313	3292	39	11.9	0.01
0.1	323	2653	167	8.0	0.37
1	323	2850	119	9.2	0.04
10	323	2992	76	10.2	0.00
0.1	333	1920	211	4.3	0.20
1	333	2211	195	5.7	0.03
10	333	2497	151	7.3	0.00

(b) PA6.6 samples

Table 4 Thermoelastic contributions $E'_{\mathcal{T}}$ and $E''_{\mathcal{T}}$ to dynamic moduli.

3.3.2 Dissipative effects

Modeling aspects The irreversible character of the deformation process is expressed by the Clausius-Duhem inequality. In the framework of DMTA tests, with the chosen set of state variables, the dissipation d can be written as

$$d = \underbrace{\sigma\dot{\varepsilon} - \frac{\partial\psi}{\partial\varepsilon}\dot{\varepsilon} - \frac{\partial\psi}{\partial\tilde{f}}\dot{\tilde{f}}}_{d_1 = w_{\mathrm{d}}^{\bullet}} - \underbrace{\frac{\vec{\mathrm{grad}}T}{T}\cdot\vec{q}}_{d_2} \geqslant 0 \tag{17}$$

where $\vec{q}$ is the heat influx vector. This dissipation is traditionally split in two terms: the intrinsic dissipation classically denoted by d_1 and the thermal dissipation d_2. In order to homogenize the notations, the intrinsic dissipation will be denoted by $w_{\mathrm{d}}^{\bullet}$ from now on. The thermal dissipation d_2 depicts the irreversibility related to the heat diffusion mechanisms. In general, the Fourier law is used to link the heat influx vector to the temperature field. Fourier's law is classically written as

$$\vec{q} = -k\,\vec{\mathrm{grad}}T \tag{18}$$

where k is the conduction tensor. In the 1D rheological context of DMTA tests, the irreversibility induced by heat diffusion has been considered via the heat losses term $\theta/\tau_{\mathrm{th}}$ presents in the simplified heat equation, Equation (12). Recall that the existence of heat losses (i.e., neither isothermal nor adiabatic test), in the presence of coupling mechanisms (e.g., thermoelasticity), leads to time effects that, during a cyclic test, contributes to form a hysteresis loop (Chrysochoos 2012). This effect was highlighted by Zener (1938) who introduced the famous concept of thermoelastic internal friction.

The intrinsic dissipation $w_{\mathrm{d}}^{\bullet}$ depicts the mechanical and microstructural irreversibility. Considering Equations (6a) and (6b) and the constancy of the variable $\tilde{f}$ for a monochromatic test, $w_{\mathrm{d}}^{\bullet}$ can be rewritten in the compact form

$$w_{\mathrm{d}}^{\bullet} = \sigma^{\mathrm{ir}}\dot{\varepsilon} = \frac{E''_{\mathcal{M}}}{\omega_0}\dot{\varepsilon}^2 = E''_{\mathcal{M}}\omega_0\varepsilon_0^2\cos^2(\omega_0 t) = E''_{\mathcal{M}}\omega_0\varepsilon_0^2\frac{1+\cos(2\omega_0 t)}{2} \geqslant 0. \tag{19}$$

This term corresponds to the part of the deformation energy rate $\sigma\dot{\varepsilon}$ that is attributed to the loss modulus. The thermodynamic analysis allows one to claim that this mechanical energy rate is dissipated and must therefore be irreversibly transformed into heat. To check the coherence of this interpretation from a dissipative standpoint with the experimental results, the following way has been chosen.

The goal is to pass from dissipation to self-heating temperature. Analogously to Equation (12), the heat diffusion equation considering the dissipative source only was rewritten as

$$\frac{\mathrm{d}\theta}{\mathrm{d}t} + \frac{\theta}{\tau_{\mathrm{th}}} = \frac{w_{\mathrm{d}}^{\bullet}}{\rho C}. \tag{20}$$

Then, using the analytic form of the intrinsic dissipation given in Equation (19), the heat equation was integrated over time to give the evolution of the corresponding thermal effects. Let us note θ_d the temperature variation, solution of Equation (20). Once the transient term vanished, we get

$$\theta_d(t) = \left(\frac{1}{2} + \frac{1}{\sqrt{1+4\omega_0^2\tau_{\mathrm{th}}^2}}\sin(2\omega_0 t + \phi_d)\right)\frac{E''_{\mathcal{M}}\varepsilon_0^2\omega_0\tau_{\mathrm{th}}}{\rho C} \quad \text{with} \quad \tan\phi_d = \frac{1}{2\omega_0\tau_{\mathrm{th}}}. \tag{21}$$

Note that, once again, a component of the thermo-signal should beat at $2f_0$. However, the weighting term in front of it tends very quickly to zero for f_0 greater than 10^{-1} Hz in the present case, and more generally when $f_0 \gg \frac{1}{4\pi\tau_{\mathrm{th}}}$.

Irrespective of f_0, the mean temperature variation θ_d stabilizes around the value

$$(\delta\theta_d^{f_0})_{\mathrm{theo}} = \frac{E''_{\mathcal{M}}\varepsilon_0^2\omega_0\tau_{\mathrm{th}}}{2\rho C} = \frac{\pi E''_{\mathcal{M}}\varepsilon_0^2\tau_{\mathrm{th}}}{\rho C} f_0. \tag{22}$$

Confrontation of experimental data with predicted ones The stabilized temperatures $(\delta\theta_d^{f_0})_{\mathrm{theo}}$ were compared to the corresponding values $(\delta\theta_d^{f_0})_{\mathrm{exp}}$ experimentally observed for each couple (T_0, f_0). Results are gathered in Tables 5(a) and 5(b) for PS and PA6.6 samples, respectively.

f_0 [Hz]	T_0 [K]	E" [MPa]	$(\delta\theta_d^{f_0})_{\mathrm{theo}}$ [mK]	$(\delta\theta_d^{f_0})_{\mathrm{exp}}$ [mK]
0.1	313	67	1	8
1	313	65	6	11
10	313	64	62	21
0.1	348	86	1	24
1	348	72	7	17
10	348	76	74	50
0.1	363	140	1	22
1	363	86	8	37
10	363	39	38	62

(a) PS samples

f_0 [Hz]	T_0 [K]	E" [MPa]	$(\delta\theta_d^{f_0})_{\mathrm{theo}}$ [mK]	$(\delta\theta_d^{f_0})_{\mathrm{exp}}$ [mK]
0.1	313	85	<1	−1
1	313	60	3	10
10	313	39	20	85
0.1	323	167	1	−15
1	323	119	6	23
10	323	76	39	143
0.1	333	211	1	−1
1	333	195	10	24
10	333	151	78	190

(b) PA6.6 samples

Table 5 Comparison of experimental and theoretical dissipation-induced self-heating.

The comparison between "theoretical" and "experimental" dissipation-induced self-heating values may appear more delicate than the one concerning thermoelastic effects. In the previous case, the synchronous demodulation technique allowed to delete almost totally the low frequency thermal noise (chamber regulation) and high frequency one (electronic noise, parasitic reflections). The temperature increases induced by dissipation seem thus much more scattered.

Partial concluding comments But then, what can we learn from the analysis of self-heating?

- The first observation made in Tables 5(a) and 5(b) is that the higher the frequency, the greater the self-heating. This property is true for all "theoretical" results, and nearly all the time for "experimental" ones, cf. Equation (4). As the loss modulus E'' decreases with f_0, it must be less quickly than f_0^{-1}, see Equation (22). Note that the simplest parallel linear viscoelastic model (i.e., the Kelvin-Voigt model), characterized by a constant viscosity with respect to f_0, imposes that E'' is a linear increasing function of f_0. Its self-heating is then proportional to f_0^2, see Appendix A.
- At $f_0 = 0.1$ Hz, the effects of noise were however visible in that negative values of $(\delta\theta_d^{f_0})_{\mathrm{exp}}$ were experimentally detected, especially in the case of PA6.6 samples.
- The self-heating $(\delta\theta_d^{f_0})_{\mathrm{exp}}$ is measured during a cyclic test of about 3 minutes (starting from a thermal equilibrium of the sample). The value of $(\delta\theta_d^{f_0})_{\mathrm{theo}}$ corresponds to the asymptotic

mean temperature reached when the average dissipation over a cycle is equal to the heat losses over this same cycle. This asymptotic temperature is then a maximum temperature. If $(\delta\theta_d^{f_0})_{\text{theo}} \geq (\delta\theta_d^{f_0})_{\text{exp}}$, one can always claim that the sample has not yet reached its maximum self-heating. However the reverse inequality, $(\delta\theta_d^{f_0})_{\text{theo}} \leq (\delta\theta_d^{f_0})_{\text{exp}}$, is more problematic and this situation occurs around two out of three times in Tables 5(a) and 5(b), what is upsetting.

- Naturally, this thermal analysis of dissipative effects can be questioned, considering that the self-heating observed here remained too weak. Using the same loading frequencies, we could have probably amplified these thermal effects by increasing the strain amplitude ε_0 which remained very low ($\varepsilon_0 = 10^{-3}$). However, it seemed important to stay within a deformation range where the linear viscoelasticity framework seems to be indisputable. We came back to this important point in the final concluding comments and in the Appendix.

3.3.3 Energy rate balance

The previous paragraphs have shown that the thermal effects induced by thermoelasticity and dissipation have comparable ranges, of the order of a hundred mK. It seemed interesting to see now what the associated heat rates correspond to. For this purpose, energy rate balances are proposed. We have chosen, this time, to show these balances for PS specimens loaded under extreme conditions, see Figure 8.

The terms defining the energy balance rate are as follows:

$$w_{\text{def}}^{\bullet} = \sigma\dot{\varepsilon} = w_{\text{e}}^{\bullet} + w_{\text{d}}^{\bullet}, \tag{23a}$$

$$w_{\text{e}}^{\bullet} = \sigma^{\text{r}}\dot{\varepsilon} = E'_{\mathcal{M}}(\varepsilon - \lambda_{\text{th}}\theta)\dot{\varepsilon} \approx \tfrac{1}{2}E'_{\mathcal{M}}\varepsilon_0^2\omega_0 \sin(2\omega_0 t), \tag{23b}$$

$$w_{\text{d}}^{\bullet} = \sigma^{\text{ir}}\dot{\varepsilon} = E''_{\mathcal{M}}\varepsilon_0^2\omega_0 \cos^2(\omega_0 t), \tag{23c}$$

$$w_{\text{the}}^{\bullet} = -\lambda_{\text{th}} T E'_{\mathcal{M}}\dot{\varepsilon} = -\lambda_{\text{th}}(T_0 + \theta)E'_{\mathcal{M}}\varepsilon_0\omega_0 \cos(\omega_0 t) \approx -\lambda_{\text{th}} T_0 E'_{\mathcal{M}}\dot{\varepsilon}. \tag{23d}$$

The deformation energy rate $w_{\text{def}}^{\bullet}$ is made of elastic $w_{\text{e}}^{\bullet}$ and dissipated $w_{\text{d}}^{\bullet}$ energy rates. We also added the thermoelastic energy rate $w_{\text{the}}^{\bullet}$, even if it does not appear in the classic DMTA. The approximation in Equations (23b) and (23d) comes from the fact that $\lambda_{\text{th}}\theta \ll \varepsilon$ and $\theta \ll T_0$, respectively.

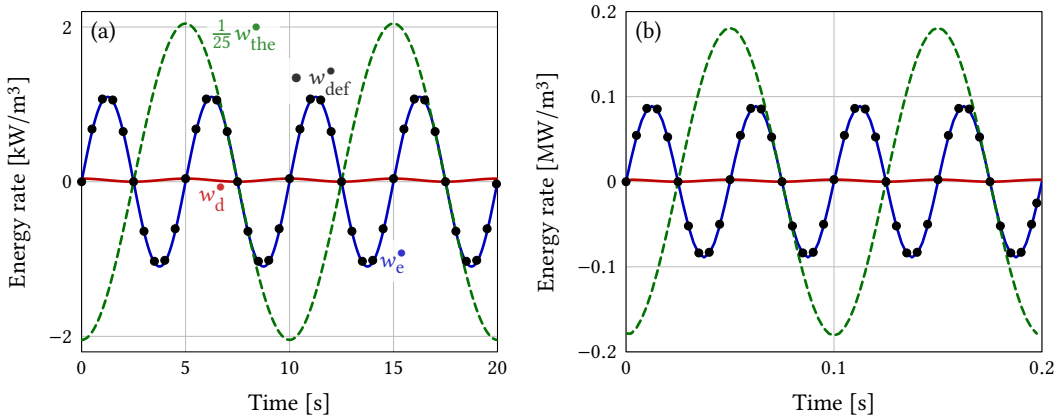

Figure 8 Energy rate balances for PS: (a) $T_0 = 313\,\text{K}$, $f_0 = 0.1\,\text{Hz}$; (b) $T_0 = 363\,\text{K}$, $f_0 = 10\,\text{Hz}$.

The first obvious result is that the thermoelastic energy rate involved in the transformation is undoubtedly the most important term of the balance. In Figure 8, it should be noted that, to make the comparison of the curves easier, the thermoelastic energy rate has been divided by 25.

The second result, equally obvious, is the extreme lowness of dissipation. The dissipation is so low that the deformation energy rate is almost identical to that of the elastic one. Nevertheless, it has been underlined that these small mechanical dissipations (always positive) generated temperature variations comparable to those induced by (alternating) thermoelastic coupling sources.

3.3.4 Hysteresis area

The energy preponderance of coupling effects led us to control the influence that their presence can have on the hysteresis loop area $\mathcal{A}_\mathrm{h}$. Using Equation (16b), we get

$$\mathcal{A}_\mathrm{h} = \int_t^{t+f_0^{-1}} \sigma(\tau)\dot{\varepsilon}(\tau)\,\mathrm{d}\tau = \pi E''\varepsilon_0^2 = \mathcal{A}_\mathrm{h}^\mathrm{d} + \mathcal{A}_\mathrm{h}^\mathrm{the} \tag{24}$$

where $\mathcal{A}_\mathrm{h}^\mathrm{d}$ and $\mathcal{A}_\mathrm{h}^\mathrm{the}$ stand for the dissipative and the thermoelastic contributions. The viscous term $\mathcal{A}_\mathrm{h}^\mathrm{d}$ is naturally defined by

$$\mathcal{A}_\mathrm{h}^\mathrm{d} = \int_t^{t+f_0^{-1}} w_\mathrm{d}^\bullet(\tau)\,\mathrm{d}\tau. \tag{25}$$

The presence of strong thermomechanical coupling mechanisms, in non-adiabatic situation, leads to time effects that contribute to the creation of a hysteresis loop. In the case of thermoelastic effects, this contribution $\mathcal{A}_\mathrm{h}^\mathrm{the}$ is written as, using Equations (11) and (13):

$$\mathcal{A}_\mathrm{h}^\mathrm{the} = \int_t^{t+f_0^{-1}} w_\mathrm{the}^\bullet\,\mathrm{d}\tau = \int_t^{t+f_0^{-1}} -E'_\mathcal{M}\lambda_\mathrm{th}\underbrace{(\delta\theta_\mathrm{e}^{f_0})_\mathrm{theo}\sin(\omega_0\tau+\phi_\mathrm{the})}_{\theta_\mathrm{the}(\tau)}\underbrace{\varepsilon_0\omega\cos(\omega_0\tau)}_{\dot{\varepsilon}(\tau)}\,\mathrm{d}\tau. \tag{26}$$

Then, after integration over time, we get:

$$\mathcal{A}_\mathrm{h}^\mathrm{the} = \frac{\pi E'_\mathcal{M}\varepsilon_0\lambda_\mathrm{th}(\delta\theta_\mathrm{e}^{f_0})_\mathrm{theo}}{\sqrt{1+\omega_0^2\tau_\mathrm{th}^2}} = \pi E''_\mathcal{T}\varepsilon_0^2. \tag{27}$$

In Tables 6(a) and 6(b), both types of hysteresis areas have been computed. The remarkable finding is that, despite the preponderance of thermoelastic effects in the energy rate balance, the contribution of these coupling effects to the creation of a hysteresis area remains negligible in the loading conditions considered here, particularly at high frequency. This is the same type of conclusion obtained when studying the influence of thermoelastic effects on the definition of dynamic moduli, see Equation (16b) and Tables 4(a) and 4(b). However, as explained in Section 3.3.1, we sought to see if coupling effects still have as little relative importance on the size of hysteresis loop at very low frequencies. In other words, at very low frequencies, is irreversibility associated with intrinsic or thermal dissipation, viscosity or material thermo-dilatability?

f_0 [Hz]	T_0 [K]	E' [MPa]	E'' [MPa]	$(\delta\theta_e^{f_0})_\mathrm{theo}$ [mK]	$\mathcal{A}_\mathrm{h}$ [J/m³]	$\mathcal{A}_\mathrm{h}^\mathrm{the}$ [J/m³]
0.1	313	3490	67	51	210	1.85
1	313	3564	65	53	205	0.19
10	313	3608	64	53	199	0.02
0.1	348	2882	86	47	269	1.40
1	348	2977	77	48	242	0.15
10	348	3046	73	50	229	0.02
0.1	363	2529	140	43	441	1.13
1	363	2673	86	46	269	0.13
10	363	2826	39	48	123	0.01

(a) PS samples

f_0 [Hz]	T_0 [K]	E' [MPa]	E'' [MPa]	$(\delta\theta_e^{f_0})_\mathrm{theo}$ [mK]	$\mathcal{A}_\mathrm{h}$ [J/m³]	$\mathcal{A}_\mathrm{h}^\mathrm{the}$ [J/m³]
0.1	313	3490	67	51	210	1.85
1	313	3564	65	53	205	0.19
10	313	3608	64	53	199	0.02
0.1	348	2882	86	47	269	1.40
1	348	2977	77	48	242	0.15
10	348	3046	73	50	229	0.02
0.1	363	2529	140	43	441	1.13
1	363	2673	86	46	269	0.13
10	363	2826	39	48	123	0.01

(b) PA6.6 samples

Table 6 Computations of the hysteresis area $\mathcal{A}_\mathrm{h}$ and $\mathcal{A}_\mathrm{h}^\mathrm{the}$ for DMTA tests.

3.3.5 Possible extrapolation to very low frequencies

Since the thermal effects at very low loading frequencies are experimentally unreachable, numerical simulations were performed using the basic visco-thermo-elastic Zener-type model illustrated in Figure 9, see also (Moreau et al. 2005). The parameters used in the simulations

Figure 9 Zener-type model.

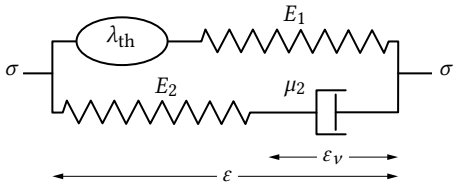

are listed in Table 7. The values of thermal expansion coefficient λ_{th}, of the mass density ρ, of the specific heat C were the ones retained for the PS samples, see Table 1. The elastic moduli E_1 and E_2 and the viscosity μ_2 were chosen to get the same hysteresis areas $\mathcal{A}_h$ and $\mathcal{A}_h^{the}$ as those obtained for the PS samples at $T_0 = 363\,K$, $f_0 = 0.1\,Hz$, see bold line in Table 8 compared to Table 6(a). We also made sure that the chosen E_1, E_2 and μ_2 give dynamic moduli that follow as well as possible their experimental evolutions with f_0 at T_0, at best only, because the euristic Zener model, which has only one thermoelastic and one viscoelastic branch, remains a rather simple model.

Parameters	E_1[MPa]	E_2[MPa]	μ_2[MPa s]	τ_2[s]	λ_{th}[10^{-6}/K]	ρ[kg/m^3]	C[J/kg/K]	τ_{th}[s]	ε_0[−]
Values	2500	620	241	0.39	75	1060	1400	40	0.01

Table 7 Model parameters in the numerical simulations.

The energies $\mathcal{A}_h$ and $\mathcal{A}_h^{the}$ were computed for different low frequencies and gathered in Table 8. As the loading frequency decreases, the contribution of thermoelastic effects to the hysteresis area $\mathcal{R} = \mathcal{A}_h^{the}/\mathcal{A}_h = E''_{\mathcal{T}}/E''$ increases. In Table 8, we see that the ratio $\mathcal{R}$ tends numerically to a limit value when the loading frequency tends to zero. An analytical calculation of the ratio, associated with the thermoelastic model of Zener-type, gives a limit value equal to

$$\lim_{f_0 \to 0} \mathcal{R} = \frac{E_1^2 \lambda_{th}^2 T_0 \tau_{th}}{E_1^2 \lambda_{th}^2 T_0 \tau_{th} + \rho C \mu_2} = 0.588. \tag{28}$$

The calculations leading to this result are detailed in Appendix B.

At very low frequencies, for the material characteristics selected here, the preponderance of the thermoelastic effects is then indisputable. This means that, at these frequencies, the loss modulus is preferentially induced by thermomechanical coupling effects associated with heat diffusion rather than viscous effects. One could introduce at this level the concept of apparent "coupling viscosity" μ_c induced by the thermo-dilatability character of the material in a non-adiabatic, non-isothermal context. At very low frequencies, the thermoelastic effects will be more important than viscous effects if the "coupling viscosity" is greater than the material viscosity:

$$\mu_c = \frac{E_1^2 \lambda_{th}^2 T_0 \tau_{th}}{\rho C} > \mu_2. \tag{29}$$

The preponderance of thermoelastic effects on dissipation is not an intrinsic characteristic of the material, but of the material, the geometry of the specimen and the conditions of heat exchange between the specimen and the environment, see the definition of τ_{th} above Equation (12). This means that the "coupling viscosity" is consequently not a "pure" material characteristic.

Finally, in Table 8, one can notice the non-monotonic evolution of $\mathcal{A}_h^{the}$ when the loading frequency f_0 increases, following a passage from isothermal (i.e., low frequencies) to adiabatic (i.e., high frequencies) processes.

4 Concluding comments

In this work, we first sought to develop an infrared set-up allowing to reach the very small temperature variations accompanying the cyclic loading of polymer samples during DMTA tests. The first important finding, in agreement with the DMTA interpretation framework, is that the

Table 8 Relative importance of thermoelastic effects at different loading frequencies, with data for PS at 0.1 Hz and 363 K used as reference.

f_0 [Hz]	$\mathcal{A}_\mathrm{h}^\mathrm{d}$ [J/m³]	$\mathcal{A}_\mathrm{h}^\mathrm{the}$ [J/m³]	$\mathcal{R}$ [%]
10^{-4}	0.47	0.68	58.7
10^{-3}	4.7	6.3	56.9
10^{-2}	47.3	9.1	16.2
10^{-1}	**441**	**1.1**	**0.25**
1	669	0.12	0.018
10^{1}	79.7	0.01	0.016
10^{2}	8.0	0.001	0.016

temperature variations of the specimen during the tests remain so small that the assumption of isothermal testing is well acceptable from a purely thermal standpoint, but not necessarily from an energy standpoint since, for solid materials (high mass density, high specific heat), a small thermal effect can reveal important energy mechanisms.

To interpret the thermomechanical results and their energy consequences, we integrated the rheological equations of the DMTA in the framework of the nonlinear TIP with internal state variables. The thermodynamic analysis of mechanical and thermal data, obtained during various loading frequencies and temperatures, led us first to justify the introduction of thermoelastic effects. As far as thermoelasticity is concerned:

(i) its temperature ranges have been of the same order of magnitude as those induced by viscous effects,

(ii) it was very largely preponderant within the energy rate balance,

(iii) but unexpectedly and fortunately its contribution to the mechanical hysteresis area remained negligible in the loading conditions experimentally considered.

However, at very low frequencies, numerical predictions from a simple Zener-type model showed that, depending on the material characteristics, the loss modulus might be preferentially attributed to coupling effects rather than viscous effects.

As for the dissipative effects:

(i) they were more difficult to observe because the intensity of dissipation remained extremely low (more than 100 times lower than the thermoelastic energy rates),

(ii) we could nevertheless highlight that the dissipation increased with the loading frequency but in a proportion lower than the ratio of the frequencies,

(iii) this last result is certainly to be refined but it agrees with the fact that the area of the mechanical hysteresis loops decreases with the loading frequency.

This result is also compatible with the predictions of the Generalized Maxwell model (Appendix C), at least if the equivalent viscosity remains a sufficiently decreasing function of the loading frequency. Indeed, if $E_1(T_0), \ldots, E_i(T_0), \ldots E_{n-1}(T_0), E_n(T_0)$ denote the elastic moduli and $\mu_1(T_0), \mu_2(T_0), \ldots, \mu_i(T_0), \ldots \mu_n(T_0)$, the viscosity coefficients of these n viscoelastic branches placed in parallel (with $E_n(T_0) = \infty$ and $\mu_1(T_0) = \infty$), it is classically shown (Ferry 1980) that the equivalent loss modulus E'' can be written as

$$E'' = \mu_\mathrm{eq}(T_0, f_0)\omega_0 \quad \text{with} \quad \mu_\mathrm{eq}(T_0, f_0) = \sum_{i=2}^{n-1} \frac{\mu_i(T_0)}{1 + \tau_i^2 \omega_0^2} + \mu_n(T_0). \tag{30}$$

where $\tau_i(T_0) = \mu_i(T_0)/E_i(T_0)$ is the relaxation time associated with branch #i. According to Equation (24), the hysteresis area is therefore $\mathcal{A}_\mathrm{h} = 2\pi^2 \varepsilon_0^2 f_0 \mu_\mathrm{eq}(T_0, f_0)$. As long as the apparent viscosity $\mu_\mathrm{eq}(T_0, f_0)$ is frequency dependent, a decay of the hysteresis area with the loading frequency is possible, but once the asymptotic value $\mu_\mathrm{eq}(T_0, f_0) = \mu_n(T_0)$ is reached, the hysteresis loop area must become an increasing linear function of f_0. It seems then difficult to interpret the near constancy of E'' observed on the PS at high frequency or low T_0 (see Figure 4). This constancy would tend to show that only the viscous (pure) branch is active and its viscosity μ_n evolving as f_0^{-1}, which is not consistent with the framework of linear viscoelasticity. This will be discussed in more detail in a future work, where we will seek to identify from the DMTA results on PS and PA6.6, a possibly non-linear generalized Maxwell model taking the thermoelasticity into account.

Appendix

The purpose of this appendix is to briefly remind some energy properties of the different viscoelastic models referred to in this work. These models must predict the DMTA rules shown in Equation (1) which claim that, at a constant temperature, a monochromatic loading (e.g., in strain) generates a (stress) response of the same spectral content. This remarkable property is generally limited to small strain where the material behavior remains linear and viscoelastic. The phase shift observed between stress and strain, Equation (1b), as well as the introduction of dynamic moduli, Equations (1c) and (1d), lead us to rewrite the stress-strain relationship in additive form, see Equation (5), where elasticity effects develop in parallel with viscous effects. This parallel character is fundamental because it strongly structures the rheological models that can be proposed. In the following we will briefly come back to the three models mentioned in this paper as well as the reasons that led us to mention them.

A Kelvin-Voigt model

This is the simplest viscoelastic parallel model, illustrated in Figure A.1. It is well suited to DMTA in that it introduces only one kinematic state variable: the overall deformation ε. In the field of linear viscoelasticity, the elasticity modulus E and the viscosity μ are constant. The stress can

Figure A.1 Kelvin-Voigt model.

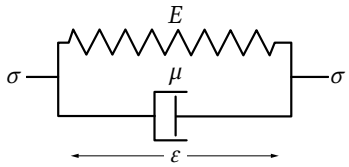

classically be written as $\sigma = \sigma^{\mathrm{r}} + \sigma^{\mathrm{ir}} = E\varepsilon + \mu\dot{\varepsilon}$. From Equations (6a) and (6b), we get the forms of the dynamic moduli $E' = E$ and $E'' = \mu\omega_0 = 2\pi\mu f_0$. In the case of the strain-driven DMTA test in Equation (1a), the associated intrinsic dissipation is $w_{\mathrm{d}}^{\bullet} = \sigma^{\mathrm{ir}}\dot{\varepsilon} = \mu\dot{\varepsilon}^2 = \frac{1}{2}\mu\omega_0^2\varepsilon_0^2(1+\cos(2\omega_0 t))$. Inserted in Equation (20), this yields the mean value of the asymptotic self-heating

$$(\delta\theta_d^{f_0})_{\mathrm{theo}} = \frac{2\pi^2\tau_{\mathrm{th}}\mu\varepsilon_0^2}{\rho C} f_0^2. \tag{A.1}$$

This self-heating is here a function of f_0^2, which is not consistent with experimental observations. This is not surprising since E'' is here an increasing function of f_0 whereas E'' was decreasing in the experimental conditions retained, see Figure 4.

In Section 3.3 to keep this parallel structure, with one kinematic state variable, we were led to admit that E and μ vary with the loading frequency, thus leaving the classical framework of linear viscoelasticity. In other words, we considered that E became $E'(T_0, f_0)$ and μ, $E''(T_0, f_0)/2\pi f_0$, see Equation (5).

B Zener-type model

Another way to describe a viscoelasticity evolving with the loading frequency, while keeping rheological parameters constant, is to increase the number of rheological elements. Thus, in Section 3.3.5, we used the Zener-type model for which the elastic branch becomes thermoelastic and the other branch, viscoelastic, introduces a viscous strain ε_v as a new state variable. Although still rudimentary, this model allowed us to analyze the relative importance of thermoelastic coupling and dissipative effects for very low loading frequencies, where calorific effects remain currently unreachable. Before analyzing the energy properties of this model, it should be noticed that, in Figure 9, the thermoelasticity only concerns the elastic branch. We could have considered both springs as thermoelastic.

This is what we formally have done in Equation (5) by attaching the thermo-dilatation to the conservation modulus only. Having only one thermoelastic component naturally simplifies the model. It also allows to find a thermoelastic temperature range independent of the frequency,

as soon as the cycle can be considered as adiabatic, which we would not have had with a viscous-thermoelastic branch, the viscous strain depending on the loading frequency. In this model, two heat sources coexist, the thermoelastic source $w^{\bullet}_{\text{the}}$ and the intrinsic dissipation $w^{\bullet}_{\text{d}}$.

- From Equation (10) with $\psi(T, \varepsilon, \varepsilon_v)$ the volume free energy, the thermoelastic source reads

$$w^{\bullet}_{\text{the}} = T\frac{\partial^2\psi}{\partial T\,\partial\varepsilon}\dot{\varepsilon} = -E_1\lambda_{\text{th}}T\dot{\varepsilon} = -E_1\lambda_{\text{th}}T_0\dot{\varepsilon} - E_1\lambda_{\text{th}}\theta\dot{\varepsilon}. \tag{B.1}$$

Given the low ratio $|\theta|/T_0$ (less than 10^{-3}), the thermoelastic temperature variations can be calculated with a good precision from the simplified source term $-E_1\lambda_{\text{th}}T_0\dot{\varepsilon}$. Attention, this does not mean that the energy rate $E_1\lambda_{\text{th}}\theta\dot{\varepsilon}$ should be neglected in the energy balance over a loading cycle, see Table 8 and equation (26), particularly at low loading frequency.

- In this new rheological assembly, the intrinsic dissipation is only associated with the dashpot and reads $w^{\bullet}_{\text{d}} = \mu_2\dot{\varepsilon}_v^2$.

Starting from the rheological equations characterizing the components, the periodic part of the viscous strain verifies

$$\varepsilon_v = \frac{\varepsilon - \tau_2\dot{\varepsilon}}{1+\omega_0^2\tau_2^2} \tag{B.2}$$

where $\tau_2 = \mu_2/E_2$ is the relaxation time of the viscoelastic branch, ε being defined by Equation (1a). We finally get

$$w^{\bullet}_{\text{d}} = \mu_2\frac{\varepsilon_0^2\omega_0^2}{(1+\omega_0^2\tau_2^2)^2}\left[\cos^2(\omega_0 t) + \omega_0\tau_2\sin(2\omega_0 t) + \omega_0^2\tau_2^2\sin^2(\omega_0 t)\right]. \tag{B.3}$$

At high frequencies, the mean dissipation per cycle saturates, becoming independent of the loading frequency, while at low frequencies, the dissipation can be approximated by a f_0 squared law

$$\lim_{\omega_0\to\infty} w^{\bullet}_{\text{d}} \approx \frac{\mu_2\varepsilon_0^2}{\tau_2^2}\sin^2(\omega_0 t) = \frac{\mu_2}{\tau_2^2}\varepsilon^2 \quad \text{and} \quad \lim_{\omega_0\to 0} w^{\bullet}_{\text{d}} \approx \mu_2\varepsilon_0^2\omega_0^2\cos^2(\omega_0 t) = \mu_2\dot{\varepsilon}^2. \tag{B.4}$$

At high frequency, the asymptotic self-heating becomes independent of f_0 and reaches the asymptotic value

$$(\delta\theta_d^{f_0})_{\text{theo}} = \frac{\tau_{\text{th}}\mu_2\varepsilon_0^2}{2\tau_2^2\rho C}. \tag{B.5}$$

At low frequencies, it is interesting to compare the size of the hysteresis loops generated by the thermoelastic effects and to compare them to those of the dissipative effects. Since the thermoelastic hysteresis area is temperature dependent (Equation (26)), this latter should be computed during a cyclic test. As usual, we do not consider the transient solution. The temperature is the solution to the heat equation

$$\dot{\theta} + \frac{\theta}{\tau_{\text{th}}} = \frac{w^{\bullet}_{\text{d}}}{\rho C} + \frac{w^{\bullet}_{\text{the}}}{\rho C} = \frac{\mu_2\dot{\varepsilon}^2}{\rho C} + \frac{E_1\lambda_{\text{th}}T_0\dot{\varepsilon}}{\rho C} = \frac{\mu_2\omega_0^2\varepsilon_0^2}{\rho C}\frac{1+\cos(2\omega_0 t)}{2} + \frac{E_1\lambda_{\text{th}}T_0\varepsilon_0\omega_0}{\rho C}\cos(\omega_0 t). \tag{B.6}$$

This ODE being linear, we can look for a particular solution for each of the two terms of the right hand member. After all calculations, we find $\theta = \theta_d + \theta_{\text{the}}$ where

$$\theta_d = \underbrace{\frac{\mu_2\tau_{\text{th}}\omega_0^2\varepsilon_0^2}{2\rho C(1+4\omega_0^2\tau_{\text{th}}^2)}}_{\#1} + \underbrace{\frac{\mu_2\tau_{\text{th}}\omega_0^2\varepsilon_0^2}{2\rho C(1+4\omega_0^2\tau_{\text{th}}^2)}\cos(2\omega_0 t)}_{\#2} + \underbrace{\frac{\mu_2\tau_{\text{th}}^2\omega_0^3\varepsilon_0^2}{2\rho C(1+4\omega_0^2\tau_{\text{th}}^2)}\sin(2\omega_0 t)}_{\#3} \tag{B.7a}$$

$$\theta_{\text{the}} = \underbrace{\frac{E_1\lambda_{\text{th}}T_0\varepsilon_0\omega_0\tau_{\text{th}}}{\rho C(1+\omega_0^2\tau_{\text{th}}^2)}\cos(\omega_0 t)}_{\#4} + \underbrace{\frac{E_1\lambda_{\text{th}}T_0\varepsilon_0\omega_0^2\tau_{\text{th}}^2}{\rho C(1+\omega_0^2\tau_{\text{th}}^2)}\sin(\omega_0 t)}_{\#5}. \tag{B.7b}$$

The thermoelastic hysteresis area is defined by

$$\mathcal{A}_{\mathrm{h}}^{\mathrm{the}} = \int_t^{t+f_0^{-1}} w_{\mathrm{the}}^{\bullet}(u)\,\mathrm{d}u = \int_t^{t+f_0^{-1}} -E_1\lambda_{\mathrm{th}}T\dot{\varepsilon}\,\mathrm{d}u = \int_t^{t+f_0^{-1}} -E_1\lambda_{\mathrm{th}}\theta\dot{\varepsilon}\,\mathrm{d}u \tag{B.8}$$

with $\dot{\varepsilon} = \varepsilon_0\omega_0\cos(\omega_0 t)$. Consequently, except term #4, all other terms vanish during the integration over a loading cycle. We then get

$$\mathcal{A}_{\mathrm{h}}^{\mathrm{the}} = \frac{E_1^2\lambda_{\mathrm{th}}^2 T_0\omega_0^2\varepsilon_0^2\tau_{\mathrm{th}}}{\rho C(1+\omega_0^2\tau_{\mathrm{th}}^2)}\frac{\pi}{\omega_0} = \frac{\pi E_1^2\lambda_{\mathrm{th}}^2 T_0\omega_0\varepsilon_0^2\tau_{\mathrm{th}}}{\rho C(1+\omega_0^2\tau_{\mathrm{th}}^2)}. \tag{B.9}$$

On the other hand, the hysteresis associated with dissipation becomes, with Equation (B.3):

$$\mathcal{A}_{\mathrm{h}}^{\mathrm{d}} = \int_t^{t+f_0^{-1}} w_{\mathrm{d}}^{\bullet}(u)\,\mathrm{d}u = \frac{\mu_2\varepsilon_0^2\omega_0^2}{(1+\omega_0^2\tau_2^2)^2}\frac{\pi}{\omega_0} + \frac{\mu_2\varepsilon_0^2\omega_0^4\tau_2^2}{(1+\omega_0^2\tau_2^2)^2}\frac{\pi}{\omega_0} = \frac{\pi\mu_2\varepsilon_0^2\omega_0}{(1+\omega_0^2\tau_2^2)}. \tag{B.10}$$

Considering low frequencies, both types of areas reach a limit:

$$\lim_{\omega_0\to 0}\mathcal{A}_{\mathrm{h}}^{\mathrm{the}} \approx \frac{\pi E_1^2\lambda_{\mathrm{th}}^2 T_0\tau_{\mathrm{th}}}{\rho C}\varepsilon_0^2\omega_0 \quad \text{and} \quad \lim_{\omega_0\to 0}\mathcal{A}_{\mathrm{h}}^{\mathrm{d}} \approx \pi\mu_2\varepsilon_0^2\omega_0. \tag{B.11}$$

We then find the ratio $\mathcal{R}$ representing the relative importance of thermoelasticity at low frequency defined in Equation (28), namely

$$\mathcal{R} = \frac{E_1^2\lambda_{\mathrm{th}}^2 T_0\tau_{\mathrm{th}}}{E_1^2\lambda_{\mathrm{th}}^2 T_0\tau_{\mathrm{th}} + \rho C\mu_2}. \tag{B.12}$$

As already mentioned, the Zener model shows only one relaxation time, which rarely allows to correctly describe the moduli evolution with frequency. To improve the performances of the modelling, it is usual to increase the number of viscoelastic branches, always placed in parallel, to get a Generalized Maxwell-type model associated with a discrete relaxation time spectrum.

C Generalized Maxwell-type model

This type of model is naturally richer as the number n of branches increases. To each viscoelastic branch i we associate a relaxation time $\tau_i = \mu_i/E_i$. It is then usual to define for each model of this type a discrete distribution of relaxation times associated with E_i modules. In Figure C.2, the branch #1 is a pure thermoelastic branch ($\mu_1 = +\infty$) and the branch #n is a pure viscous branch ($E_n = +\infty$).

Figure C.2 Generalized Maxwell-type model.

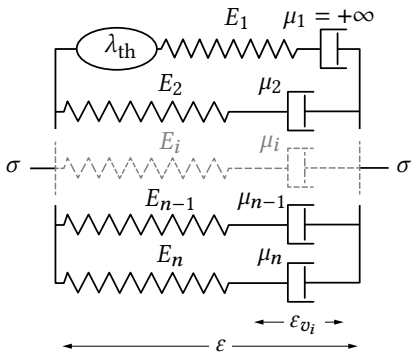

Noting $\psi(T, \varepsilon, \varepsilon_{v_i})$, $i = 1, \ldots, n$, the volume free energy, the thermoelastic source keeps the same form as in Equation (B.1), namely:

$$w_{\mathrm{the}}^{\bullet} = T\frac{\partial^2\psi}{\partial T\partial\varepsilon}\dot{\varepsilon} = -E_1\lambda_{\mathrm{th}}T\dot{\varepsilon}. \tag{C.1}$$

As before, the thermoelasticity is localised in a single branch and not distributed over the n branches of the model.

The intrinsic dissipation $w_{\mathrm{d}}^{\bullet}$ must now consider the contribution of all dashpots, that is

$$w_{\mathrm{d}}^{\bullet} = \sum_{i=2}^{n-1} \mu_i \dot{\varepsilon}_{v_i}^2 + \mu_n \dot{\varepsilon}^2. \tag{C.2}$$

For each viscoelastic branch, the periodic part of the viscous strain ε_{v_i} satisfies

$$\varepsilon_{v_i} = \frac{\varepsilon - \tau_i \dot{\varepsilon}}{1 + \omega_0^2 \tau_i^2}. \tag{C.3}$$

Following the same approach as in Equation (B.3), $w_{\mathrm{d}}^{\bullet}$ is written as

$$w_{\mathrm{d}}^{\bullet} = \sum_{i=2}^{n-1} \frac{\mu_i \varepsilon_0^2 \omega_0^2}{(1 + \omega_0^2 \tau_i^2)^2} [\cos^2(\omega_0 t) + \omega_0 \tau_i \sin(2\omega_0 t) + \omega_0^2 \tau_i^2 \sin^2(\omega_0 t)] + \mu_n \varepsilon_0^2 \omega_0^2 \cos^2(\omega_0 t). \tag{C.4}$$

As with the Zener-type model, we can calculate the limits of the dissipation at high and low frequencies:

$$\lim_{\omega_0 \to \infty} w_{\mathrm{d}}^{\bullet} \approx \sum_{i=2}^{n-1} \frac{\mu_i}{\tau_i^2} \varepsilon^2 + \mu_n \dot{\varepsilon}^2 \quad \text{and} \quad \lim_{\omega_0 \to 0} w_{\mathrm{d}}^{\bullet} \approx \sum_{i=2}^{n} \mu_i \dot{\varepsilon}^2. \tag{C.5}$$

At high frequencies, the dissipation is composed of two terms. The first, as in the Zener-type model, becomes independent of frequency, and the second, as in the Kelvin-Voigt model, sees the dissipation grow in f_0 squared because of the n^{th} branch. One could of course not consider this purely viscous branch in the model, but then this would lead to a decrease towards zero of the loss moduli E'', which is not observed (e.g. Figure 4). Indeed, it is classical to check that the dynamic moduli can be written as (Aklonis and Mac Knight 1983)

$$E' = E_1 + \sum_{i=2}^{n-1} E_i \frac{\omega_0^2 \tau_i^2}{1 + \omega_0^2 \tau_i^2} \quad \text{and} \quad E'' = \sum_{i=2}^{n-1} E_i \frac{\omega_0 \tau_i}{1 + \omega_0^2 \tau_i^2} + \omega_0 \mu_n \tag{C.6}$$

where $0 \leqslant \tau_i = \mu_i / E_i \leqslant +\infty$, $i = 1, \ldots, n$, are the relaxation times.

D On the transition from 1D to 3D viscothermoelastic models

From a modeling standpoint, the transition to a 3D thermoelasticity does not involve any new concept for isotropic materials and 3D linear thermoelastic models have been proposed for a long time (Germain 1973). Regarding now the viscosity, it is a different matter when it comes to defining and identifying the tensors characterizing the viscous properties. Naturally, 3D linear models could fit easily into the thermodynamic framework. The reader interested in this domain is referred to Sidoroff's famous website [http://sitasido.ec-lyon.fr/mainToC.php]. However, it must be clear that once defined, the viscous behavior will need a large amount of specific experimental data to be identified. In any case, we have pointed out that these linear models in their 1D version were not completely satisfactory from an energy standpoint.

References

Achorn, P. J. and R. G. Ferrillo (1994). Comparison of thermal techniques for glass transition measurements of polystyrene and cross-linked acrylic polyurethane films. *Journal of Applied Polymer Science* 54 (13):2033–2043. [DOI].

Aklonis, J. and W. Mac Knight (1983). *Introduction to Polymer Viscoelasticity*. 2nd ed. Wiley. ISBN: 9780471867296.

Batsale, J.-C., A. Chrysochoos, H. Pron, and B. Wattrisse (2013). Thermographic analysis of material behaviors. *Full-Field Measurements and Identification in Solid Mechanics*. Wiley. Chap. 16, pp 439–468. [DOI], [HAL].

Batzer, H. and U. Kreibich (1981). Influence of water on thermal transitions in natural polymers and synthetic polyamides. *Polymer Bulletin* 5(11-12):585–590. [doi].

Benaarbia, A., A. Chrysochoos, and G. Robert (2016). Thermomechanical analysis of the onset of strain concentration zones in wet polyamide 6.6 subjected to cyclic loading. *Mechanics of Materials* 99:9–25. [doi], [hal].

Boulanger, T., A. Chrysochoos, C. Mabru, and A. Galtier (2004). Calorimetric analysis of dissipative and thermoelastic effects associated with the fatigue behavior of steels. *International Journal of Fatigue* 26 (3):221–229. [doi], [hal].

Chrysochoos, A. (2012). Thermomechanical analysis of the cyclic behavior of materials. *Procedia IUTAM* 4:15–26. [doi], [oa].

Chrysochoos, A. and H. Louche (2000). An infrared image processing to analyse the calorific effects accompanying strain localisation. *International Journal of Engineering Science* 38 (16):1759–1788. [doi], [hal].

Dulieu-Barton, J. M. and P. Stanley (1998). Development and applications of thermoelastic stress analysis. *The Journal of Strain Analysis for Engineering Design* 33 (2):93–104. [doi].

Fabre, V., G. Quandalle, N. Billon, and S. Cantournet (2018). Time-Temperature-Water content equivalence on dynamic mechanical response of polyamide 6,6. *Polymer* 137:22–29. [doi], [hal].

Ferry, J. (1980). *Viscoelastic Properties of Polymers*. 3rd ed. Wiley. isbn: 9780471048947.

Germain, P. (1973). *Cours de Mécanique de Milieux Continus*. Masson. isbn: 9782225359378.

Germain, P., Q. S. Nguyen, and P. Suquet (1983). Continuum thermodynamics. *Journal of Applied Mechanics* 50 (4b):1010–1020. [doi].

Graessley, W. W. and L. J. Fetters (2001). Thermoelasticity of Polymer Networks. *Macromolecules* 34 (20):7147–7151. [doi], [oa].

Halphen, B. and Q. S. Nguyen (1975). Sur les matériaux standard généralisés. *Journal de Mécanique* 14 (1):39–63. [hal].

Honorat, V., S. Moreau, J.-M. Muracciole, B. Wattrisse, and A. Chrysochoos (2005). Calorimetric analysis of polymer behaviour using a pixel calibration of an IRFPA camera. *Quantitative InfraRed Thermography Journal* 2 (2):153–171. [doi], [hal].

Launay, A., Y. Marco, M. Maitournam, and I. Raoult (2013). Modelling the influence of temperature and relative humidity on the time-dependent mechanical behaviour of a short glass fibre reinforced polyamide. *Mechanics of Materials* 56:1–10. [doi], [hal].

Menard, K. P. (2008). *Dynamic Mechanical Analysis: A Practical Introduction*. 2nd ed. CRC Press. [doi].

Moreau, S., A. Chrysochoos, J.-M. Muracciole, and B. Wattrisse (2005). Analysis of thermoelastic effects accompanying the deformation of PMMA and PC polymers. *Comptes Rendus Mécanique* 333 (8):648–653. [doi], [hal].

Olusanya, A. (1996). A comparison of techniques for monitoring the cure of adhesives. *National Physical Laboratory Report CMMT (B)*, 104.

Reimschuessel, H. K. (1978). Relationships on the effect of water on glass transition temperature and Young's modulus of Nylon 6. *Journal of Polymer Science: Polymer Chemistry Edition* 16(6):1229–1236. [doi].

Rieger, J. (2001). The glass transition temperature $\mathcal{T}_g$ of polymers—comparison of the values from differential thermal analysis (DTA, DSC) and dynamic mechanical measurements (torsion pendulum). *Polymer Testing* 20 (2):199–204. [doi].

Rittel, D. (2000). An investigation of the heat generated during cyclic loading of two glassy polymers. Part I: Experimental. *Mechanics of Materials* 32 (3):131–147. [doi].

Sokolov, A. and Y. Hayashi (2007). Breakdown of time-temperature superposition: From experiment to the coupling model and beyond. *Journal of Non-Crystalline Solids* 353 (41):3838–3844. [doi].

Treloar, L. (2005). *The Physics of Rubber Elasticity*. 3rd ed. Oxford University Press. isbn: 9780191523304.

Wattrisse, B., A. Chrysochoos, J.-M. Muracciole, and M. Némoz-Gaillard (2001). Analysis of strain localization during tensile tests by digital image correlation. *Experimental Mechanics* 41(1):29–39. [doi], [hal].

Yadav, P. (2019). Time and thermo-mechanical coupling effects in polymers. PhD thesis. France:

Université de Montpellier. [hal].
Zener, C. (1938). Internal friction in solids II. General theory of thermoelastic internal friction. *Physical Review* 53 (1):90–99. [doi], [hal].

Authors' contributions André Chrysochoos: writing – original draft, review & editing; methodology; data processing; thermomechanical modelling; numerical modelling and simulation; supervision. Olivier Arnould: writing – review, editing & formatting of the article and figures; experimental supervision, investigation and metrology; data processing.

Supplementary Material The datasets of the fully corrected DMTA measurements for the two polymers, the average temperature variation of the sample measured by the IRFPA camera and the program (Matlab® software, MathWorks Inc., Natick, Massachusetts, USA) used for the simulation of the thermomechanical response of a Zener-type rheological model are freely available at the permalink https://doi.org/10.5281/zenodo.7257481.

Acknowledgements The authors are grateful to S. Castagnet (CNRS, Université de Poitiers, ISAE ENSMA, Poitiers, France) for fruitful discussions and her friendly support, P. Yadav (LMGC, Université de Montpellier, CNRS, Montpellier, France) for his help during the testing campaign, G. Robert (Solvay Engineering Plastics, Lyon, France) for providing the PA6.6 samples, J.J. Robin (ICGM, Université de Montpellier, CNRS, Montpellier, France) with whom we conducted our first DMTA tests and DSC measurements and N. Le Moigne (PCH, IMT Mines Ales, Ales, France), S. Corn (LMGC, IMT Mines Ales, Ales, France) and V. Placet (FEMTO-ST Institute, Université Bourgogne Franche-Comté, Besançon, France) for the DMTA comparative test campaign.

Ethics approval and consent to participate Not applicable.

Consent for publication Not applicable.

Competing interests The authors declare that they have no competing interests.

Journal's Note JTCAM remains neutral with regard to the content of the publication and institutional affiliations.